2003

Topographically driven groundwater flow and the San Andreas heat flow paradox revisited

Demian M. Saffer
University of Wyoming

Barbara A. Bekins
U.S. Geological Survey

Stephen Hickman
U.S. Geological Survey

JOURNAL OF GEOPHYSICAL RESEARCH, VOL. 108, NO. B5, 2274, doi:10.1029/2002JB001849, 2003

Topographically driven groundwater flow and the San Andreas heat flow paradox revisited

Demian M. Saffer
Department of Geology and Geophysics, University of Wyoming, Laramie, Wyoming, USA

Barbara A. Bekins and Stephen Hickman
U.S. Geological Survey, Menlo Park, California, USA

Received 28 February 2002; revised 30 December 2002; accepted 27 January 2003; published 24 May 2003.

[1] Evidence for a weak San Andreas Fault includes (1) borehole heat flow measurements that show no evidence for a frictionally generated heat flow anomaly and (2) the inferred orientation of σ_1 nearly perpendicular to the fault trace. Interpretations of the stress orientation data remain controversial, at least in close proximity to the fault, leading some researchers to hypothesize that the San Andreas Fault is, in fact, strong and that its thermal signature may be removed or redistributed by topographically driven groundwater flow in areas of rugged topography, such as typify the San Andreas Fault system. To evaluate this scenario, we use a steady state, two-dimensional model of coupled heat and fluid flow within cross sections oriented perpendicular to the fault and to the primary regional topography. Our results show that existing heat flow data near Parkfield, California, do not readily discriminate between the expected thermal signature of a strong fault and that of a weak fault. In contrast, for a wide range of groundwater flow scenarios in the Mojave Desert, models that include frictional heat generation along a strong fault are inconsistent with existing heat flow data, suggesting that the San Andreas Fault at this location is indeed weak. In both areas, comparison of modeling results and heat flow data suggest that advective redistribution of heat is minimal. The robust results for the Mojave region demonstrate that topographically driven groundwater flow, at least in two dimensions, is inadequate to obscure the frictionally generated heat flow anomaly from a strong fault. However, our results do not preclude the possibility of transient advective heat transport associated with earthquakes. *INDEX TERMS:* 8110 Tectonophysics: Continental tectonics—general (0905); 8130 Tectonophysics: Heat generation and transport; 8150 Tectonophysics: Plate boundary—general (3040); 1878 Hydrology: Water/energy interactions;
KEYWORDS: San Andreas fault, Parkfield, Mojave, heat flow, groundwater flow, heat advection

Citation: Saffer, D. M., B. A. Bekins, and S. Hickman, Topographically driven groundwater flow and the San Andreas heat flow paradox revisited, *J. Geophys. Res.*, 108(B5), 2274, doi:10.1029/2002JB001849, 2003.

1. Introduction

[2] A large body of geophysical and geological evidence has been interpreted to argue that many plate boundary faults, in both subduction zones and transform fault settings, slip at remarkably low levels of shear stress (see review by *Hickman* [1991]). These low shear stresses are in contrast to the high stress levels predicted by simple, laboratory-derived friction laws (i.e., laws assuming coefficients of friction of 0.6–1.0 and hydrostatic fluid pressures [after *Byerlee*, 1978]) and the high levels of shear stress typically supported by faults in intraplate settings [e.g., *Townend and Zoback*, 2000]. Analyses of borehole stress measurements and earthquake focal mechanisms indicate that the maximum principal stress, σ_1, is orientated at high angles (>75°) to the San Andreas Fault (SAF) along much of its length [e.g., *Zoback et al.*, 1987; *Mount and Suppe*, 1987; *Jones*, 1988; *Oppenheimer et al.*, 1988; *Zoback and Beroza*, 1993; *Townend and Zoback*, 2001]. This suggests that the San Andreas is weak in a relative sense, in that it supports considerably lower shear stresses than the surrounding crust (i.e., the SAF is a weak fault in an otherwise strong crust). However, recent inversion of earthquake focal mechanisms in southern California [*Hardebeck and Hauksson*, 1999] indicates that σ_1 may locally rotate to a more acute angle (40–60°) to the San Andreas Fault within about 10–20 km of the fault, at least in the "Big Bend" region near Fort Tejon. Although the validity of this interpretation has been challenged [*Townend and Zoback*, 2001], this apparent near-field rotation in σ_1 was interpreted by *Scholz* [2000] to indicate that both the San Andreas Fault and the adjacent crust are similarly strong. Thus until more detailed information on the state of stress immediately adjacent to the San Andreas Fault becomes available, it is clear that the implications of earthquake focal mechanisms and other

0148-0227/03/2002JB001849$09.00

stress direction indicators for the strength of the San Andreas Fault, at least in southern California, will remain controversial.

[3] As first noted by *Brune et al.* [1969] [see also *Lachenbruch and Sass*, 1973], the absence of a detectable frictionally generated heat flow anomaly associated with the SAF suggests that the absolute levels of shear stress opposing slip on the fault are very low. In a detailed analysis of this problem, *Lachenbruch and Sass* [1980] demonstrated that for the case of flat topography, conductive heat flow, a long-term average slip rate of 3.1 cm yr^{-1}, a coefficient of friction consistent with laboratory experimental data, and effective normal stresses appropriate for hydrostatic pore pressures throughout the seismogenic crust, near-surface heat flow should be elevated by $\sim$40 mW m^{-2} (1 HFU) close to a vertical San Andreas fault. In contrast, heat flow data collected from numerous shallow (mostly <250 m) boreholes along the San Andreas show no indication of such a fault-centered heat flow anomaly [*Brune et al.*, 1969; *Lachenbruch and Sass*, 1973, 1980]. More recent heat flow measurements in a 3.5-km-deep borehole located 4.2 km from the SAF at Cajon Pass, when corrected for erosional effects, radiogenic heat production and topographic refraction, confirm these earlier conclusions [*Lachenbruch and Sass*, 1992; *Lachenbruch et al.*, 1995; *Sass et al.*, 1992]. Thus heat flow measurements in shallow boreholes and the deep Cajon Pass borehole suggest that the SAF is weak in an absolute sense, in that shear tractions on the fault are considerably lower than expected for hydrostatic pore pressure and experimentally determined friction coefficients.

[4] One central issue in interpreting the heat flow data as an indicator of fault strength has been understanding and quantifying the effect of groundwater flow on redistributing or removing frictionally generated heat from a strong fault, for realistic topography, permeabilities, and boundary conditions [e.g., *O'Neil and Hanks*, 1980; *Williams and Narisimhan*, 1989; *Scholz*, 2000]. In particular, both *O'Neil and Hanks* [1980] and *Scholz* [2000] suggested that a strong SAF would be permitted if groundwater flow obscured the expected thermal signal. *Lachenbruch and Sass* [1980] showed that the heat discharged by thermal springs (discharge temperature > 15°C above annual air temperature) located within 10 km of the San Andreas trace constitutes less than 1% of the predicted frictional heat generation for a strong fault. They concluded that such focused discharge could not account for the missing heat, but raised the possibility that lower temperature fluid discharge distributed over a broad region could alter the thermal expression of a strong fault.

[5] Previous modeling work has shown that, in general, permeabilities > 10^{-17} m^2 are necessary for fluid advection to significantly perturb subsurface temperatures, for a variety of flow configurations and driving mechanisms [e.g., *Bredehoeft and Papadopulos*, 1965; *Smith and Chapman*, 1983]. *Williams and Narisimhan* [1989] showed that along the San Andreas Fault, for a wide range of permeability structures, fluid flow driven by thermal buoyancy alone (i.e., lateral heating by frictionally generated heat on the SAF) either has an insignificant effect on near-surface heat flow, or tends to accentuate a frictionally generated thermal anomaly. *Williams and Narisimhan* [1989] also found that for certain boundary conditions and permeabilities, topographically driven groundwater flow could remove a frictionally generated heat flow anomaly. However, *Williams and Narisimhan* [1989] used topographic profiles of very limited spatial extent, which effectively allowed heat to be carried across the (hydrologically open) vertical boundaries of their model by topographically driven groundwater flow. Thus their modeling results do not examine the ultimate fate of frictionally generated heat along the SAF (if it exists) and whether or not a more dispersed anomaly would be detectable by surface heat flow measurements.

[6] Here, we revisit this issue and quantify the effects of topographically driven groundwater flow on near-surface heat flow along the SAF, by incorporating realistic topographic driving potentials, boundary conditions, and a range of permeability structures. We use a two-dimensional numerical model of coupled groundwater flow and heat transport within a series of cross sections perpendicular to the San Andreas Fault in the Parkfield and Mojave regions (Figure 1), to (1) evaluate the effects of topography on conductive heat flow, (2) determine if existing heat flow data can distinguish between frictional heating predicted by strong fault and weak fault models, and (3) determine if existing heat flow data can distinguish between advection- and conduction-dominated thermal regimes. We focus specifically on testing the hypothesis that steady state, topographically driven groundwater flow could appreciably alter the near-surface expression of frictional heating along a strong fault, to an extent that existing heat flow data could be consistent with a strong SAF. As discussed below, the topographic cross sections used in our model were sufficiently long (80–120 km) relative to the anticipated scale of topographically driven groundwater flow to simulate the fate of any frictionally generated heat that might be associated with the SAF.

2. Geologic Setting and Background

[7] In both the Parkfield region of central California and the Mojave Desert in southern California, there is significant topography associated with the SAF (Figures 1–2). At Parkfield, the topography is characterized by ridges and valleys subparallel to the fault trace with relief of $\sim$1500 m, and the fault itself is located in a small rift valley off center of the topographic symmetry axis (Figures 1–2). Parkfield is characterized by highly variable lithology and complex structural juxtaposition of rock units, both to the northeast and southwest of the SAF (see *Sass et al.* [1997] for summary). The uppermost few hundred meters are composed of a variety of sedimentary rocks, metamorphic rocks, extrusive volcanics, igneous intrusive rocks, and serpentinite. Microseismicity [e.g., *Hill et al.*, 1990], magnetotelluric data [*Unsworth et al.*, 2000], and active and passive seismic studies at Parkfield [e.g., *Thurber et al.*, 1997], indicate that the fault is vertical. The Parkfield region is characterized by moderate ($M \sim 6$) earthquakes with a recurrence interval of $\sim$22 years, and also marks the transition from a locked segment of the San Andreas to the southeast to a creeping segment to the northwest. Mean heat flow over the Coast Ranges in this region is 78 mW m^{-2} [*Lachenbruch and Sass*, 1980], and these values drop off dramatically to $\sim$40 mW m^{-2} in the Central Valley to the northeast. Heat flow

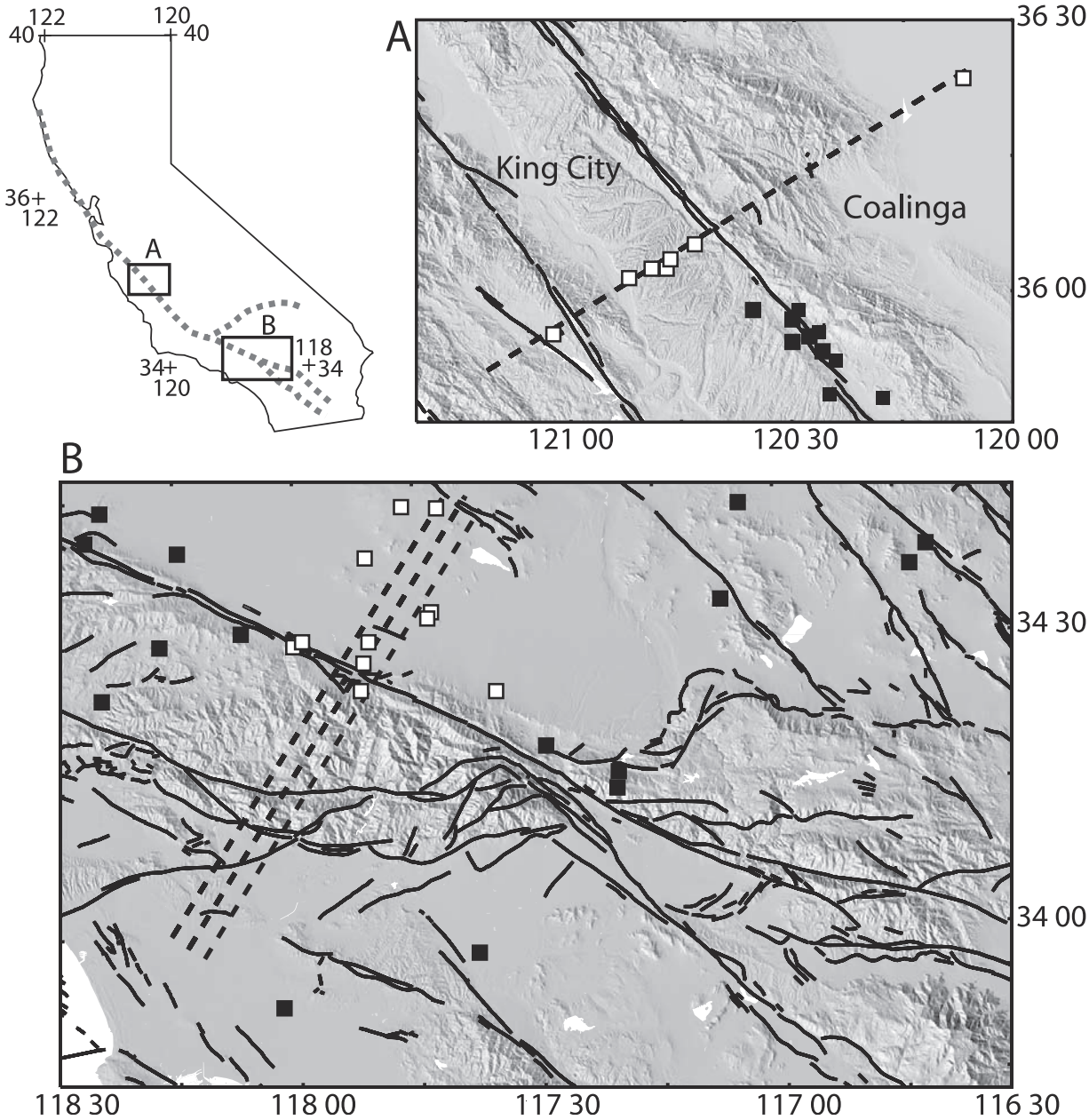

Figure 1. Shaded relief maps of (a) Parkfield and (b) Mojave study areas. Locations of each study area are shown in inset. Dashed lines show model cross sections, solid black lines are faults, and heat flow observations used in this study are shown as white squares. Other heat flow observations in each region are shown as black squares.

measurements from Parkfield used in this study were made at depths from 120 to 870 m, with all but one measurement shallower than 280 m (C. Williams, U.S. Geological Survey, personal communication, 2001).

[8] In the Mojave study area, the SAF is located along the northeastern flank of the San Gabriel Mountains (Figures 1–2). The major topographic features are subparallel to the fault trace, with relief of ~2500 m. The Mojave area is characterized mainly by igneous rocks, overlain by variable thicknesses of sedimentary basin fill to the northeast of the fault trace. The basin fill materials are typically composed of interbedded poorly consolidated clay, silt, sand, and gravel [*Galloway et al.*, 1998]. A number of studies in the region suggest that the fault is vertical [e.g., *Fuis et al.*, 2001]; however, available evidence does not exclude the possibility that along some of its length, the fault dips steeply (~75°) to the southwest beneath the San Gabriel Mountains [e.g., *Griscom and Jachens*, 1990]. This segment of the San Andreas fault is locked, and last ruptured in the 1857 M 7.8 Fort Tejon earthquake [*Ellsworth*, 1990]. Mean heat flow in this region is 63 mW m^{-2}, and is remarkably consistent over a large area [e.g., *Lachenbruch and Sass*, 1980]. Heat flow measurements used in this study were made at depths ranging from 107–1067 m (Table 1) [*Sass et al.*, 1986]. In general (and where possible), heat flow stations are sited in areas of moderate elevation,

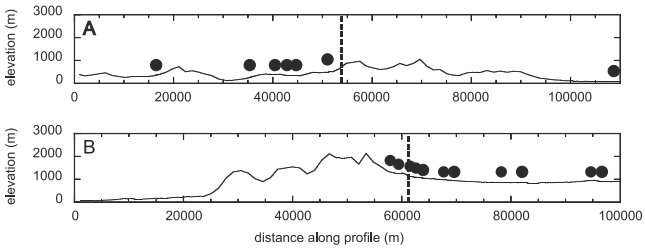

Figure 2. Topographic profiles for (a) Parkfield and (b) Mojave areas, as shown in Figures 1a and 1b, respectively. The profile for the Mojave study area is the central profile shown in Figure 1b. The locations of heat flow stations, projected onto the profile, are shown as black circles.

relatively flat topography, and in crystalline rock to avoid hydrologic and topographic effects on heat flow. The effects of uplift and erosion on measured heat flow in these areas have been discussed by *Sass et al.* [1997], *Lachenbruch and Sass* [1992], and *Lachenbruch et al.* [1995], and are generally thought to be small.

3. Methods

[9] We use a two-dimensional numerical model of steady state coupled fluid flow and heat transport along a series of profiles perpendicular to both the regional topography and the San Andreas Fault (Figures 1–3). The profiles range in length from 80 from 120 km, with end points defined by locations of regional groundwater divides. The top of the model domain is defined by the actual topography, sampled at 1.5 km spacing from USGS digital elevation models. We fix the water table at the topographic surface and specify a uniform surface temperature of 10°C. Our preliminary modeling results show that incorporating an atmospheric lapse rate of 6°C km^{-1} at the top boundary affects the modeled temperature field, but has only a minimal effect on modeled heat flow (generally <1 mW m^{-2}).

[10] The lateral model boundaries are closed to fluid and heat flow in most simulations. In some simulations, we explore the effects of an open lateral boundary by specifying hydrostatic pressure and conductive temperatures at the lateral model boundaries. The basal boundary is located at 10 km below sea level, and is closed to fluid flow, with a specified heat flux defined by the regional average near-surface heat flow [*Lachenbruch and Sass*, 1980; *Sass et al.*, 1997]. We treat the fault itself as an embedded line source of heat [e.g., *Lachenbruch and Sass*, 1980]. We assume that the fault is vertical at Parkfield and consider both a vertical fault and one that dips southwest at 75° to evaluate the thermal effects of a steeply dipping fault in the Mojave.

[11] We consider cases for frictional heating along (1) a strong fault that acts as a heat source increasing linearly with depth by 8.85 mW m^{-2} per km defined assuming a fault-parallel shear stress gradient of 9 MPa km^{-1} and a long-term average slip rate of 3.1 cm yr^{-1}, and (2) a weak fault that acts as a heat source of 1.97 mW m^{-2} per km defined by a shear stress gradient of 2 MPa km^{-1}, which achieves an average shear traction along the fault of 10 MPa within the model domain, as suggested for a depth-averaged shear stress along a weak SAF by *Lachenbruch and Sass* [1980]. We solve the coupled fluid flow and heat transport equations using the finite element code SUTRA [*Voss*, 1984]. Model outputs include pore pressure and temperature throughout the model domain, and fluid and heat fluxes across the model boundaries. To evaluate models, we compare near-surface conductive heat flow calculated over the upper few hundred meters of the model domain with observed heat flow, which is generally obtained from measured thermal gradients within the upper few hundred meters.

[12] Typically, heat flow data are corrected for the conductive effects of local topography out to distances of 2–5 km from the measurement well [e.g., *Sass et al.*, 1997; *Birch*, 1950; C. Williams, U.S. Geological Survey, personal communication, 2000]. The magnitude of the heat flow correction is generally 0–10% [e.g., *Sass et al.*, 1997] and typically decreases with distance from the borehole, although the magnitude of heat flow correction at distances of 3–5 km may be significant if large topographic gradients exist [e.g., *Birch*, 1950]. Other uncertainties in comparing heat flow data and model results include the effects of thermal refraction across subsurface lithologic discontinuities, and terrain effects such as slope orientation and vegetation cover, all of which influence heat flow data but are not included in our models [e.g., *Sass et al.*, 1997; *Blackwell et al.*, 1980]. To facilitate comparison between heat flow data and model results, we have included error bars of ±15% on all heat flow observations to account for the uncertainties noted above [e.g., *Sass et al.*, 1997]. We consider this 15% range as a probable upper bound to the uncertainty in comparing model results and observations because (1) most heat flow corrections are less than ~5% [e.g., *Sass et al.*, 1997] (for example, the smooth topography northeast of the San Andreas Fault in the Mojave study area should result in a relatively small correction) and (2) the 1.5 km topographic sampling we use for our models is comparable to the distance over which much of the topographic heat flow correction is applied. However, because the magnitude of slope orientation and vegetation effects are poorly characterized and can approach several

Table 1. Heat Flow Stations From the Mojave Study Area[a]

Station	Depth, m	Heat Flow, mW m^{-2}	Lithology
Pear Blossom (LTTM)	197	56	andesite
Palmdale Stress 'A' (DPB)	238	63	sandstone
Chief Paduke, (SC-4, US4)	238	65	shale and sandstone
Little Rock (LTTM)	296	62	granite
Palmdale Stress 'B'	243	65	crystalline
Palmdale Stress 'B2'	265	74	crystalline
Virginia Lee, (SC-5, US5)	256	74	Shale & sandstone
Phelan, SC-6	1067	63	sediments
Black Butte	654	69	crystalline
Palmdale Stress 'C'	219	63	crystalline
Palmdale Stress 'D'	195	66	crystalline
Hi Vista	107	67	crystalline
Hi Vista	610	65	crystalline
Hi Vista, South Observation Well	184	64	crystalline
Palmdale Stress 'E'	224	69	crystalline

[a]Station name, depth of heat flow determination, observed heat flow, and lithology (lithology data from *Sass et al.* [1986] and C. Williams (personal communication, 2001)) are given. Stations are ordered according to location, from SW to NE on the profiles shown in Figures 2b, 4c, 4d, 5b, and 6.

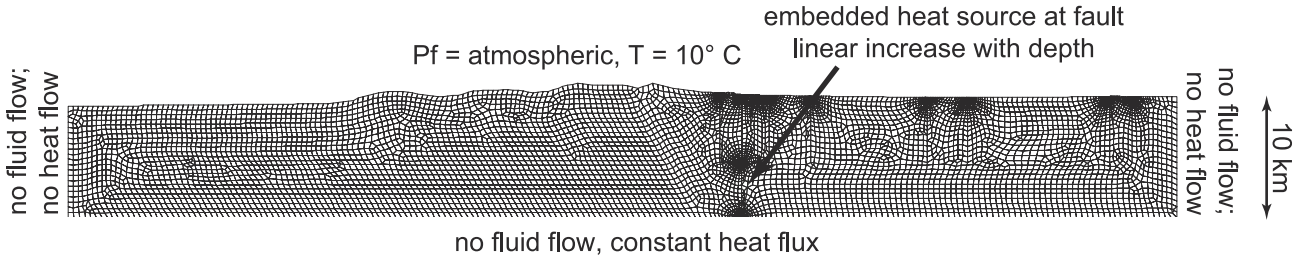

Figure 3. Example model domain showing finite element grid and boundary conditions. The model domain extends to 10 km below sea level.

percent in some cases [e.g., *Blackwell et al.*, 1980], we use an uncertainty of ±15% for all data points.

[13] In both the Mojave and Parkfield areas, we selected model cross sections to come as close as possible to a significant number (7–11) of heat flow measurements at varying distances from the SAF (Figure 1). In the Parkfield area, several heat flow determinations within a few km of the fault trace lie ~10–30 km southeast of our profile, but no heat flow data at greater distances from the SAF are available there (Figure 1a) [*Sass et al.*, 1997]. We include these data in our evaluation of models, but note that they are projected along strike for several kilometers. In the Mojave, we evaluate the effects of topographic variability along strike by considering a series of parallel cross sections separated along strike by ~5 km (Figure 1b). This approach is also useful in interpreting our model results using the heat flow data, because heat flow observations are often presented by collapsing the data into a single profile [e.g., *Lachenbruch and Sass*, 1980].

[14] We investigate several groundwater flow scenarios. In the simplest case, permeability is homogeneous and isotropic throughout the model domain. In other cases permeability varies systematically with depth, based on the analysis of *Ingebritsen and Manning* [1999]:

$$\log k_{xx} = -14 - 3.2 \log z$$
$$k_{zz} = k_{xx}/10 \quad (1)$$

where k_{xx} is horizontal permeability in m^2, k_{zz} is vertical permeability, and z is depth in km. The combination of active thrusts, active ancillary strike-slip faults, and potentially rotated structures throughout the crust surrounding the San Andreas [e.g., *Scholz*, 2000], probably results in a complex regional-scale permeability structure, with multiple and spatially variable orientations for enhanced permeability. Thus we do not explicitly evaluate the effects of potential regional-scale permeability anisotropy caused by fracture networks here.

[15] To evaluate the effects of altered permeability near the fault zone, we explore three cases: (1) a 2-km-wide high-permeability damage zone surrounding the fault with a permeability of 10^{-13} m^2; (2) a 2-km-wide damage zone with a permeability of 10^{-15} m^2; and (3) a low-permeability barrier in the fault core with a permeability of 10^{-20} m^2. We also explore the effects of a fault zone that acts as a combined conduit barrier, for a fault composed of a low-permeability gouge core ($k = 10^{-20}$ m^2) surrounded by a high-permeability damage zone composed of fractured country rock ($k = 10^{-13}$ m^2) [e.g., *Caine et al.*, 1996]. In all of these scenarios, we evaluate the case where permeability in the surrounding crust is defined by equation (1), and also the case where the surrounding crust is homogeneous, with a permeability of 10^{-15} m^2 (the highest value for homogeneous permeability explored in our simulations). By assigning a high regional permeability in the latter set of simulations, we evaluate the maximum effect of fault permeability structure on regional heat flow [e.g., *Smith and Chapman*, 1983].

[16] Finally, we approximate the effects of fluid loss by discharge into active shallow groundwater basins and subsequent down-valley (along-strike) heat and fluid movement, by relaxing the no-flow lateral boundary condition (Figure 3). In these simulations, we assign a conductive geothermal gradient and hydrostatic pore pressure at the lateral boundaries.

[17] It is important to recognize that in many mountainous areas, the water table configuration is poorly constrained, owing to a scarcity of wells at high elevation or in bedrock [e.g., *Forster and Smith*, 1988]. We note that in the Parkfield area, well water levels generally lie within 0–100 m of the land surface, even at ridge tops (F. Riley, U.S. Geological Survey, personal communication, 2000). By assigning the water table at the topographic surface, we evaluate the maximum effect of topographically driven groundwater flow on regional heat flow patterns for each permeability scenario; if groundwater flow is recharge limited, the resulting decreased water table relief would drive smaller groundwater fluxes and have smaller effects on subsurface temperatures [e.g., *Forster and Smith*, 1988].

4. Model Results and Discussion

4.1. General Patterns of Heat Flow

[18] In all simulations, modeled heat flow varies considerably with topography. For homogeneous permeabilities $<10^{-17}$ m^2 (results are not shown), modeled heat flow is indistinguishable from the results for a homogeneous permeability of 10^{-17} m^2. Thus we consider model simulations for homogeneous permeability of 10^{-17} m^2 to be dominated by conduction. In such conduction-dominated cases, heat flow is depressed at topographic highs and elevated at topographic lows. For both the Parkfield and Mojave areas, conductive heat flow exhibits scatter of ±15 mW m^{-2} due to topographic variations at wavelengths greater than the 3–5 km for which data are typically corrected (Figures 4a–4e, blue curves). However, the thermal signal from frictional heating along a strong fault is distinguishable from that for a weak fault in

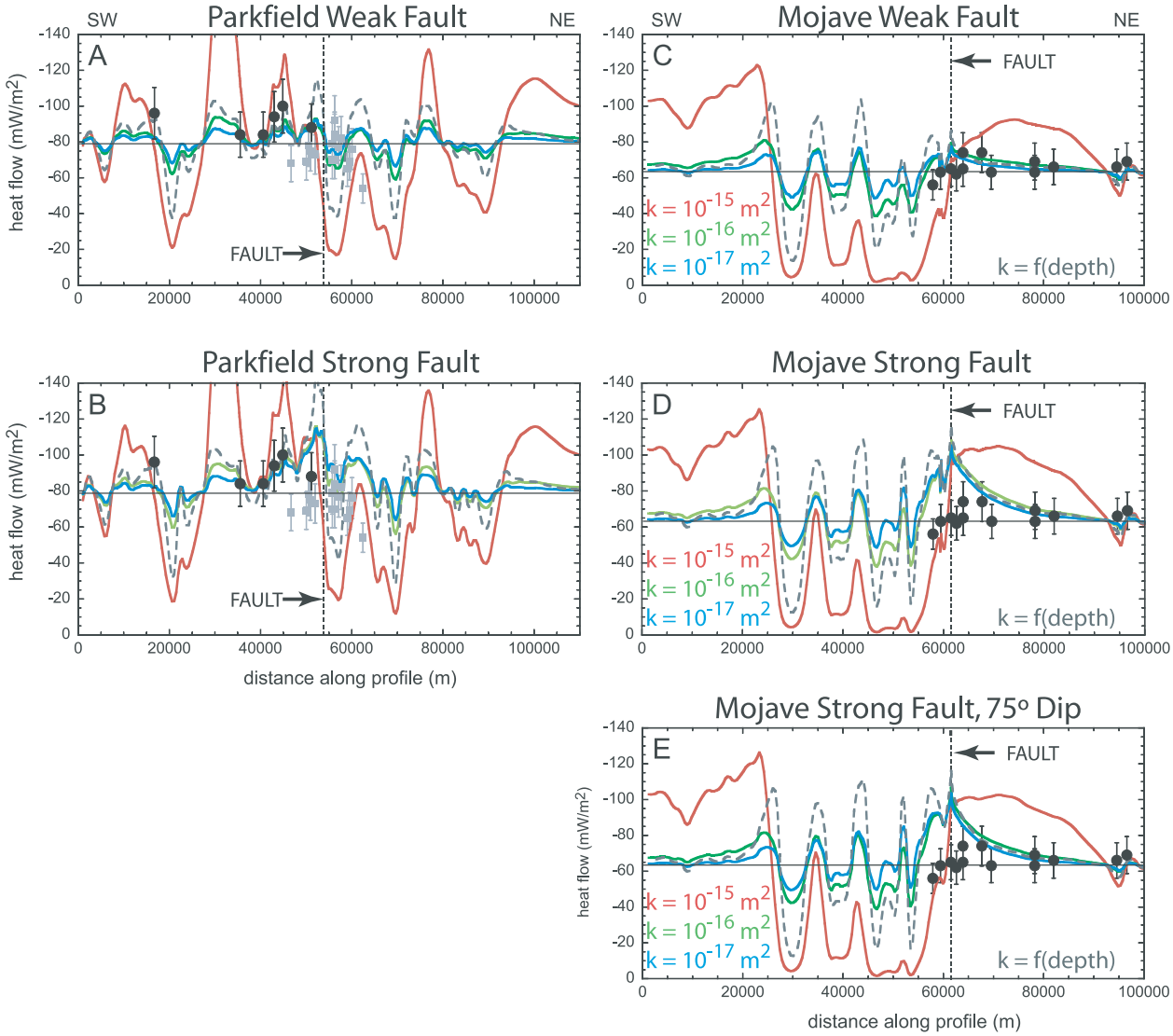

Figure 4. Modeled surface heat flow for several scenarios in the Parkfield and Mojave study areas, using homogeneous permeabilities of 10^{-15} m^2 (red curves), 10^{-16} m^2 (green curves), 10^{-17} m^2 (blue curves), and depth-varying permeability described by equation (1) (dashed gray curves). Heat flow data projected from within <5 km onto the model section are shown by black solid circles, and the thin black line indicates the regional average heat flow specified across the model base. At Parkfield, heat flow data projected from ~10–30 km to the southeast [from *Sass et al.*, 1997] are shown by gray solid squares. Error bars of ±15% on heat flow observations represent uncertainty in comparing data and model results due to topographic corrections to heat flow data and uncertainties in thermal conductivity [e.g., *Sass et al.*, 1999] The vertical dotted black line in each figure shows the fault location. (a) Parkfield profile, as shown in Figure 1, for a weak fault. (b) Parkfield profile, for a strong fault. (c) Central profile in the Mojave region, as shown in Figure 1, for a weak fault. (d) Central profile in the Mojave region for a strong fault. (e) Central profile in the Mojave region for a strong fault, dipping 75° to the southwest.

both areas, albeit slightly modified from the idealized conductive model of *Lachenbruch and Sass* [1980] because of surface topography. As expected, the conductive heat flow signal from a strong fault is modified most in areas of rugged topography, such as the areas southwest of the fault trace in the Mojave and northeast of the fault trace in Parkfield (see Figures 1a–1b).

[19] The pattern of depressed heat flow at topographic highs and elevated heat flow at topographic lows seen in the purely conductive cases is strongly accentuated by groundwater flow, as shown by model results for permeabilities of 10^{-16} to 10^{-15} m^2. For homogeneous permeability of 10^{-15} m^2, maximum modeled heat flow values are 180 mW m^{-2} at Parkfield and 125 mW m^{-2} in the Mojave; minimum values are 14 mW m^{-2} at Parkfield (Figures 4a–4b, red curves) and 0 mW m^{-2} in the Mojave (Figures 4c–4e, red curves). In such high-permeability simulations, maximum modeled recharge rates in the topographically high portions of our models are 3–5 cm yr^{-1}, which is 7–10% of the mean annual precipitation measured at high elevation

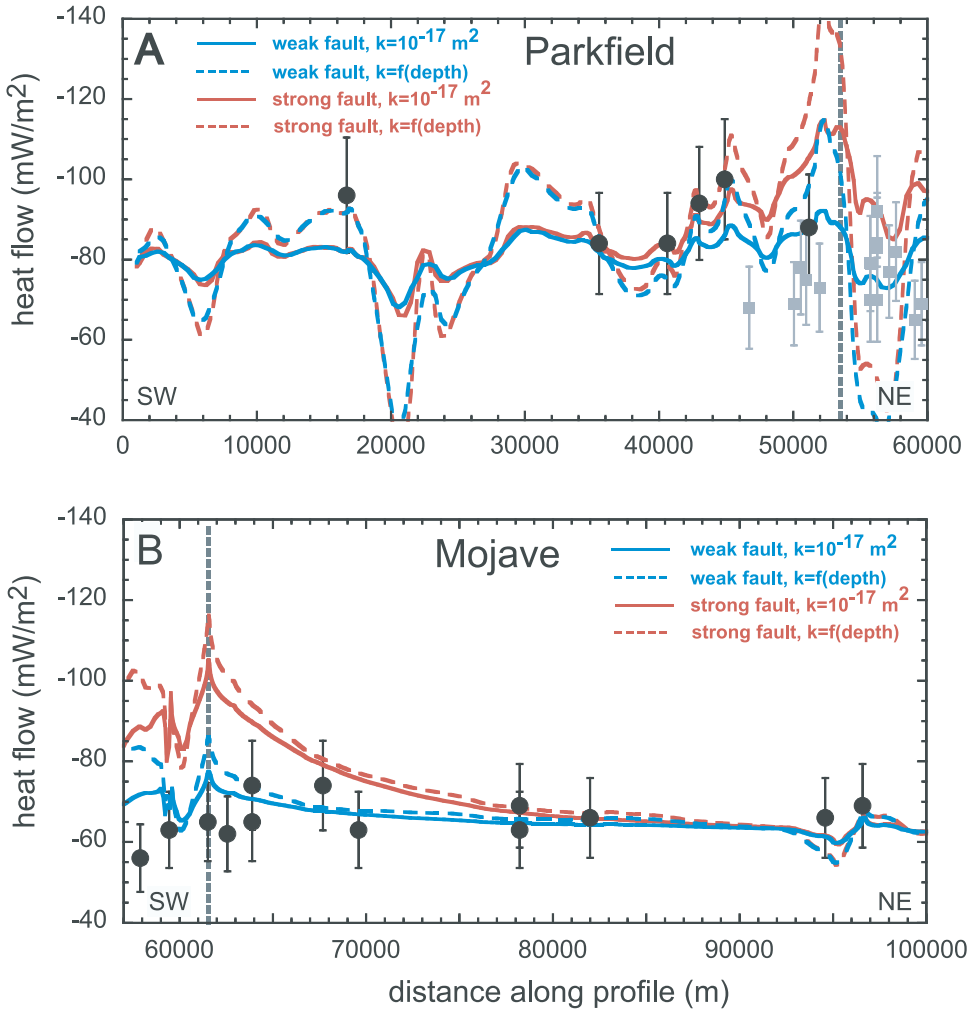

Figure 5. Enlarged plot of heat flow for (a) Parkfield and (b) Mojave profiles, showing model results for a strong (red curves) and weak (blue curves) San Andreas Fault. Fault location is indicated by vertical gray dashed line. Results are shown for two hydrologic scenarios: a conductively dominated thermal regime ($k = 10^{-17}$ m^2, solid curves), and one in which permeability decreases with depth according to equation (1). Heat flow data are projected from <5 km along strike (black circles) and from ~10–30 km to the southeast (gray solid squares) onto the model section, with ±15% error bars as discussed in text.

recharge areas in central and southern California [*Planert and Williams*, 1995]. Although difficult to measure accurately, actual recharge rates in environments characterized by water deficits (where annual potential evaporative losses exceed annual precipitation), such as the California Coast Ranges and Western Transverse Ranges [e.g., *Planert and Williams*, 1995], are typically less than a few percent of annual precipitation [e.g., *Durbin*, 1978]. Thus the high infiltration rates required by our high-permeability simulations suggest that such a model overestimates the actual rates of topographically driven groundwater flow.

[20] In the case of anisotropic permeability that decreases with depth as defined by equation (1), modeled surface heat flow departs significantly from the conduction-dominated case in areas of rugged topography where local flow systems dominate, but does not differ from conductive models in areas where regional groundwater discharge (or upward flow in the subsurface) occurs (dashed gray line, Figures 4a–4e). In regions of rugged topography in the uppermost, high-permeability areas, the magnitude of advective disturbance lies between those for homogeneous permeabilities of 10^{-15} m^2 and 10^{-16} m^2. These results are generally consistent with those of *Smith and Chapman* [1983], who demonstrated that the effects of regional groundwater flow on surface heat flow increase with the depth extent of high permeability zones.

[21] The thermal signal of a steeply dipping (75°) fault in the Mojave is indistinguishable from that for a vertical fault, for both conduction and advection-dominated heat transport. (Figures 4d–4e). This result is consistent with analytic solutions for conductive heat transport, which demonstrate that the shape of a near-surface heat flow anomaly generated by frictional heating is insensitive to the depth distribution of heat generation along the fault [e.g., *Lachenbruch and Sass*, 1980].

4.2. Advection of Frictionally Generated Heat

[22] For the Parkfield region, models that incorporate frictional heating from both a strong and weak fault are

consistent with the distribution of observed heat flow, for a wide range of permeabilities (Figures 4a–4b). At Parkfield, most of the heat flow observations along the profile are southwest of the fault trace (Figures 4a–4b, black solid circles), where short wavelength, rugged topography leads to significant along-profile variations in heat flow for the highest permeability assumed. As a result, given the differences in model predictions for the advection-dominated and the conduction-dominated cases, and accounting for the uncertainty associated with heat flow determinations and corrections for local topography, the existing data along the transect do not distinguish between our strong and weak fault models, or between advection- or conduction-dominated heat transport. The single heat flow measurement 3 km southwest of the SAF is more consistent with either conductive or advective heat transport and heating from a weak fault than with heating from a strong fault. However, the heat flow data 8 and 12 km southwest of the fault seem equally consistent with an advectively disturbed weak fault heating model or a primarily conductive strong fault heating model. The heat flow station at the northeastern edge of the Parkfield profile is located beyond the eastern edge of the Coast Range province, and heat flow there is considerably lower (46 mW m^{-2}) than the regional average for the Coast Range province. The heat flow data from *Sass et al.* [1997] projected from ~10–30 km to the southeast (Figures 4a–4b and 5a, gray solid squares) exhibit significant scatter, and are consistent with models for primarily conductive heat transport and heat production along either a strong or a weak fault. To the southwest of the fault trace, the projected heat flow values are slightly lower than any modeled values. Following *Sass et al.* [1997], we suggest that the generally lower and more scattered heat flow values to the southeast are related to variations in regional background heat flow along strike of the SAF.

[23] In the Mojave region, model results for heating along a weak fault provide a reasonable match to heat flow data for a wide range of permeabilities (Figure 4c). These models include homogeneous permeabilities of 10^{-16} m^2 or less or variable permeability described by equation (1). For higher permeabilities, modeled heat flow is elevated along the northeasternmost 40 km of the model profile by a component of upward regional groundwater flow in areas of low elevation, and exceeds observed heat flow by 20–25 mW m^{-2} over most of this region.

[24] In contrast, models that incorporate frictional heating from a strong fault yield heat flow values that are inconsistent with observations in the Mojave region, for any of the permeability structures we investigated (Figure 4d). In all cases, our strong-fault heating models predict elevated heat flow to the northeast of the fault trace, and observations are as much as 40 mW m^{-2} less than modeled values (Figure 4d). For homogeneous permeabilities of 10^{-16} m^2 or less, and for variable permeability, modeled heat flow to the northeast of the fault is similar to that predicted by the purely conductive model of *Lachenbruch and Sass* [1980]. These low-and variable-permeability model results cannot match observed heat flow near the fault, where the thermal signature of a strong SAF should be most pronounced, but can match the data at distances greater than 15 km from the fault. High permeabilities accentuate this misfit, in that model results for a homogeneous permeability of 10^{-15} m^2 differ significantly from observed heat flow both near the fault trace and at distances up to 30 km away (and downslope) where regional groundwater discharge occurs.

[25] For a steeply dipping fault, for permeabilities of 10^{-15} m^2, 10^{-16} m^2, and for depth-varying permeability (Figure 4e), modeled near-surface heat flow is nearly identical to that for a vertical fault (Figure 4d). As noted above, for conduction-dominated heat transport, the near-surface heat flow pattern is insensitive to the depth distribution of heat generation along the fault [e.g., *Lachenbruch and Sass*, 1980]. For cases of where advective heat transport is significant, the near-surface heat flow pattern is dominantly controlled by groundwater recharge and discharge, with little influence from the embedded line source of heat at depth (Figures 4d–4e, red curves).

[26] When viewed in greater detail, it is clear that existing heat flow observations do not readily distinguish between frictional heating from a strong versus a weak fault at Parkfield (Figure 5a) but are inconsistent with heat production on a strong fault in the Mojave (Figure 5b). Heat flow observations at Parkfield are consistent with heat production on a weak fault for both conduction-dominated ($k = 10^{-17}$ m^2) and variable permeability (k defined by equation (1)) scenarios (Figure 5a, blue curves). Observations are also consistent with heat generation on a strong fault for these hydrologic scenarios over most of the model domain (red curves), with the exception of the northeasternmost data point. In contrast, heat flow data in the Mojave clearly distinguish between models (Figure 5b). Even when accounting for the uncertainty in comparing model results with corrected heat flow data, heat flow predicted for a strong fault is consistently higher than observed values at distances of 8 km or less from the fault trace. Modeled heat flow for a weak SAF is generally consistent with observed heat flow values, along the entire profile. To the southwest and adjacent to the fault, modeled heat flow values are slightly higher than observations. This discrepancy could be explained by (1) projection of heat flow data into a single profile in areas characterized by along-strike topographic variability (see Figures 1b and 6a), (2) an even smaller amount of frictional heating along the fault (~1.5 MPa km^{-1}), or (3) local fluid flow in this region.

[27] We further explore the validity of our results for the Mojave profile by evaluating the viability of a strong fault model for several additional scenarios. In analyzing heat flow data or comparing data to modeled results, observations are often collapsed into a single profile across the fault [e.g., *Lachenbruch and Sass*, 1980]. We evaluate the effects of along-strike topographic variability by computing modeled heat flow for the three Mojave desert profiles shown in Figure 1, and collapsing them onto a single profile (Figures 6a–6b). Modeled along-strike variability in heat flow is generally <20 mW m^{-2}, and <10 mW m^{-2} northeast of the fault trace, an area characterized by smooth topography. Even accounting for along-strike variability in heat flow caused by topographic variations, it is clear that results from the strong fault heating model are inconsistent with heat flow observations (Figure 6b).

[28] To evaluate the possibility of large-scale fluid and heat loss by discharge into active shallow groundwater basins to the southwest or northeast of our model domain and subsequent down-valley (along-strike) flow, we open

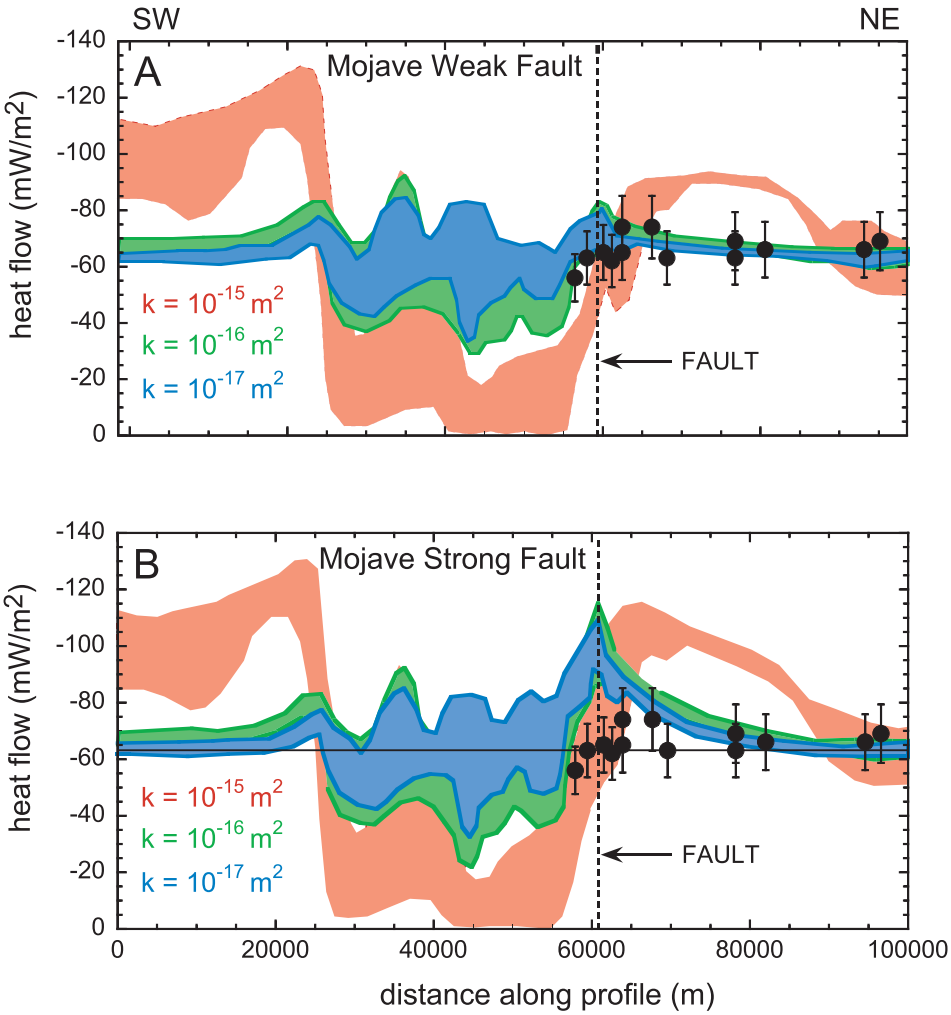

Figure 6. Range of modeled surface heat flow for the three model profiles in the Mojave region shown in Figure 1b, for homogeneous permeabilities of 10^{-15} m^2 (red shaded area), 10^{-16} m^2 (green shaded area), 10^{-17} m^2 (blue shaded area), for (a) heat generation along a weak fault and (b) heat generation along a strong fault. Note that the variation in modeled heat flow along strike is small, especially to the NE of the fault. Model results for heating along a weak fault are consistent with observations, whereas results for heating along a strong fault are not.

the lateral model boundaries to fluid and heat flow. For the scenarios we explored, a homogeneous permeability of 10^{-15} m^2 results in the largest effect on heat flow, decreasing modeled values by <5 mW m^{-2} from the case where lateral boundaries are specified as no flow (compare Figures 7 and 4d). The effect is limited to the region fs <15 km from the boundary (Figure 7). The magnitude of this effect is <2 mW m^{-2} for homogeneous permeability of 10^{-17} m^2 and for variable permeability. Although not a comprehensive investigation of potential mechanisms for strike-parallel fluid and heat transport, our results suggest that such a mechanism is unlikely to obscure a frictionally generated thermal anomaly. The Mojave region, northeast of the San Andreas Fault trace, is characterized by bedded basin fill sediments of variable thickness, with potentially strong formation-scale hydraulic anisotropy [e.g., *Galloway et al.*, 1998]. Although such anisotropy could guide significant subhorizontal fluid and heat movement both within and perpendicular to our cross sectional models, we note that most heat flow stations in this area are sited in crystalline rocks either at outcrops or where valley fill is thin (Table 1). Thus even vigorous fluid flow and heat advection within overlying and adjacent valley fill should have little impact on observed or modeled heat flow in the crystalline basement.

4.3. Effects of Fault Zone Permeability Structure

[29] More complex permeability structures within the SAF zone, in which a low-permeability fault core acts as a barrier to flow or a high-permeability damage zone acts as a conduit, yield distinct modeled heat flow patterns (Figures 8a–8c). A low-permeability core has little effect on surface heat flow for the case where country rock permeability decreases with depth as defined by equation (1), when compared with models that do not include a fault zone with separate hydrologic properties (Figures 8a–8b, solid curves; Figures 4c–4d; gray curves). This is true regardless of the magnitude of frictional heat generation

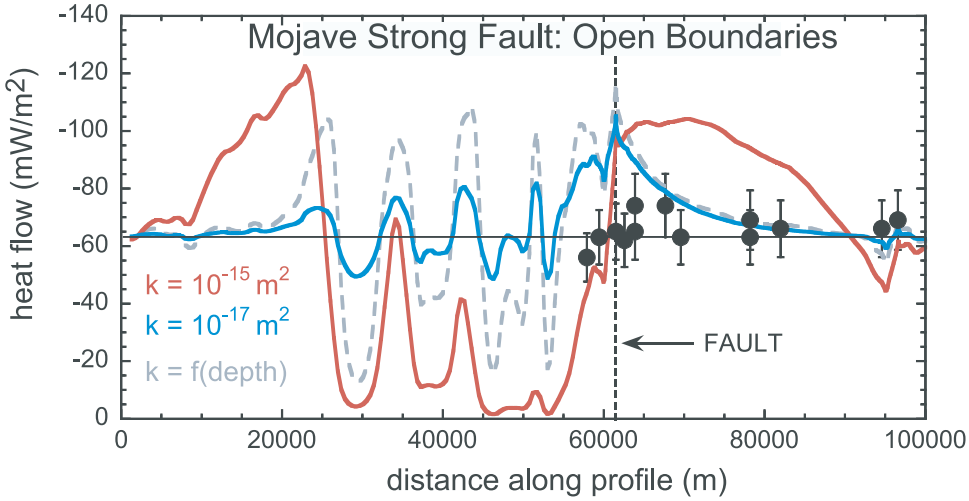

Figure 7. Model results for the central Mojave profile shown in Figure 1b, for the case where lateral boundaries are open to fluid flow, for permeabilities of 10^{-15} m^2 (red curve), 10^{-17} m^2 (blue curve), and defined by equation (1) (gray dashed curve).

(Figures 8a–8b). A high-permeability ($k = 10^{-13}$ m^2) damage zone results in large variations in heat flow within the highly permeable region for both frictional heating scenarios (weak and strong fault). In both cases, there is a minimum value near 0 mW m^{-2} up gradient (SW) of the damage zone where fluids are accessed, and a maximum value of >200 mW m^{-2} where fluids discharge from the damage zone (Figures 8a–8b, short-dashed curves). Maximum modeled fluid discharge in this scenario is ~1.75 m yr^{-1}, and its location is coincident with the maximum in heat flow; maximum downflow is ~2.2 m yr^{-1}, and occurs at the minimum in heat flow. These values locally exceed estimated recharge rates for the area by a factor of ~200. A moderate-permeability damage zone ($k = 10^{-15}$ m^2) results in a pattern of surface heat flow intermediate between the high- and low-permeability fault zone models, with slightly decreased heat flow up gradient (SW) of the damage zone, and slightly increased heat flow within it (Figures 8a–8b, dashed line with open circles). A combined conduit barrier fault affects heat flow in the same way as a high-permeability conduit but decreases the magnitude of variability in modeled heat flow within and just up gradient of the damage zone by a factor of ~2 (not shown).

[30] For all fault zone permeability scenarios we examined, heat flow is not affected appreciably outside of a narrow window approximately ~2–4 km wide (Figures 8a–8b). To the southwest of the fault, a high-permeability damage zone depresses heat flow and could be consistent with frictional heat generation along a strong fault (Figure 8b, curve for $k = 10^{-13}$ m^2) or along a weak fault (Figure 8a, curves for $k = 10^{-13}$ m^2 and $k = 10^{-15}$ m^2). However, to the northeast of the fault, for frictional heat generation on a strong fault, neither high nor low fault permeability models are consistent with observed heat flow (Figure 8b, all curves). In contrast, fault conduit and barrier models that incorporate a weak fault thermal signal are both generally consistent with heat flow data (Figure 8a, curves for $k = 10^{-15}$ m^2 and $k = 10^{-20}$ m^2).

[31] The heat flow data do not provide tight constraints on fault zone hydrologic properties. A range of damage zone permeabilities from 10^{-15} m^2 to $<10^{-20}$ m^2, or combined conduit barrier fault zone models with damage zone permeabilities $\leq 10^{-15}$ m^2 yield modeled heat flow values that are consistent with observed heat flow for frictional heating along a weak fault (Figure 8a). Damage zone permeabilities $>10^{-15}$ m^2 may also be permitted, because the large fluctuations in heat flow predicted for such scenarios would only be observed if heat flow observations were sited within an extremely narrow zone on or near the fault trace or within such fractured rocks. Few existing springs are located along or near the fault trace [e.g., *Kharaka et al.*, 1999], suggesting that a continuous, highly permeable damage zone is probably not realistic. The fact that large variations in heat flow are generally not observed at the fault trace [e.g., *Lachenbruch and Sass*, 1980; *Sass et al.*, 1997] also suggests that regionally, such a highly permeable damage zone probably does not dominate hydrology and heat transfer. The detailed fault zone hydrology could be better constrained by heat flow measurements specifically targeted at the damage zone.

[32] In order to evaluate the maximum effect that a high- or low-permeability fault zone could have on the heat flow pattern generated by frictional heating along a strong fault, we consider the case where country rock permeability is homogeneous at 10^{-15} m^2 [e.g., *Smith and Chapman*, 1983] (Figure 8c). A low-permeability fault zone results in depressed heat flow over a region extending ~8 km to the northeast of the fault trace, because regional groundwater flow across the fault is reduced (Figure 8c, solid curve). In this portion of the profile, modeled heat flow for a fault barrier model and frictional heating along a strong fault is consistent with observed heat flow. However, the fault barrier model also predicts elevated heat flow in a region extending ~6 km to the southwest of the fault trace, where the low-permeability fault redirects northeastward regional groundwater flow. Here, modeled heat flow is 80–100 mW m^{-2} greater than observed. For a high-permeability (10^{-13} m^2) damage zone, modeled heat flow is depressed over a region extending >10 km to the southwest of the fault trace, because the fault increases regional

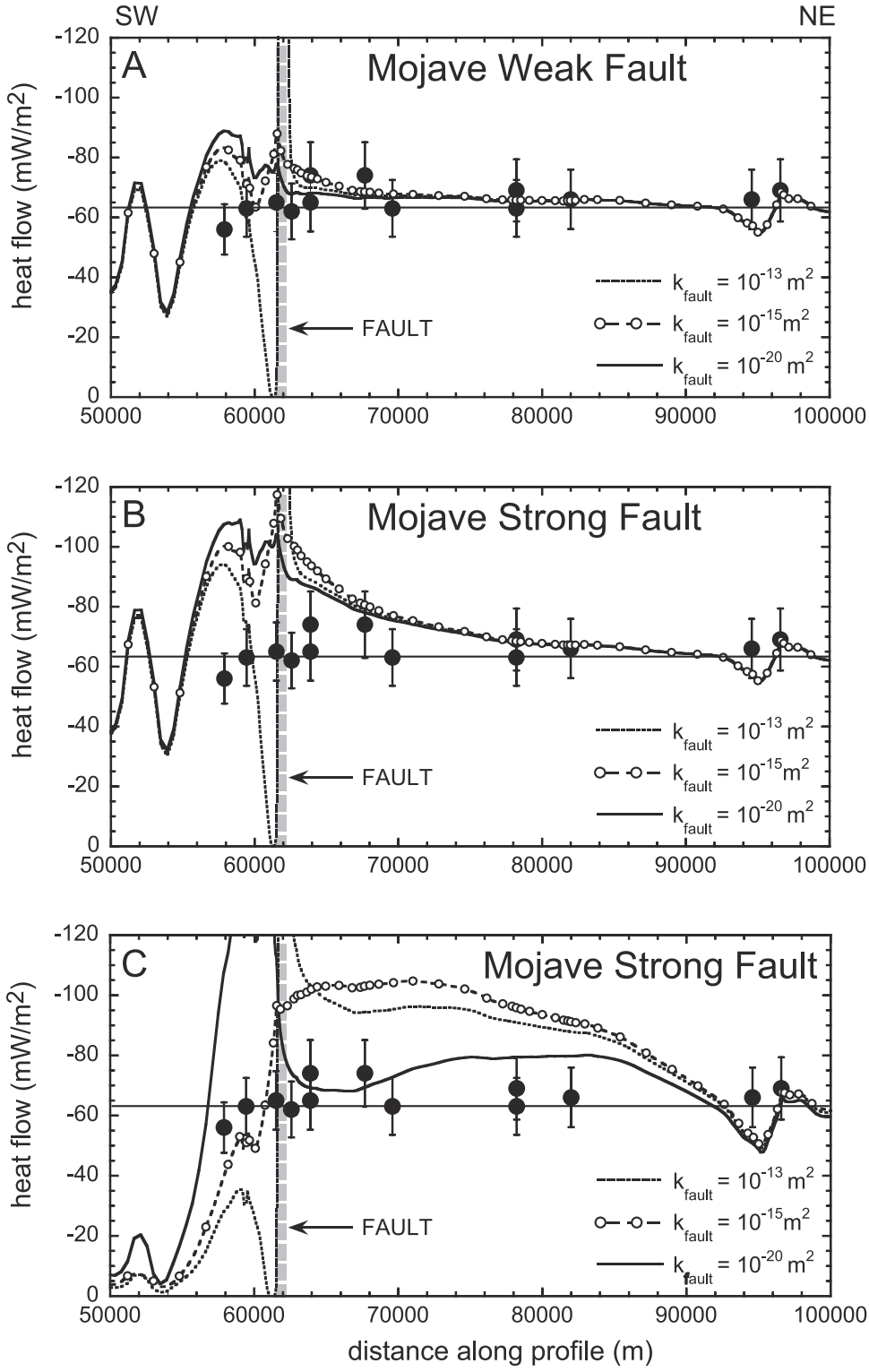

Figure 8. Modeled surface heat flow along the central Mojave profile for fault zone (area shown by gray shading) permeabilities of 10^{-13} m^2 (short-dashed curve), 10^{-15} m^2 (dashed curve with open circles) and 10^{-20} m^2 (solid curve), for (a) frictional heating for a weak fault model, with country rock permeability decreasing with depth as defined by equation (1), (b) frictional heating for a strong fault model, also with country rock permeability defined by equation (1), and (c) frictional heating for a strong fault model, with a homogeneous country rock permeability of 10^{-15} m^2.

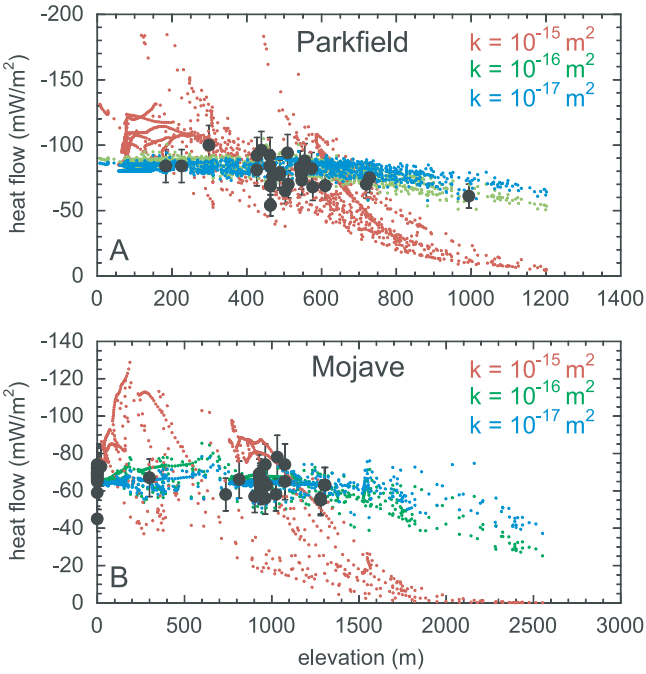

Figure 9. Modeled and observed heat flow versus elevation for (a) the Parkfield region and (b) the Mojave region. Modeled heat flow is shown for permeabilities of 10^{-15} m^2 (red circles), 10^{-16} m^2 (green circles), and 10^{-17} m^2 (blue circles). Heat flow data from all of the heat flow stations shown in Figures 1a–1b are shown by black solid circles. Note the predicted trend of decreased heat flow with increased elevation for model simulations with high permeability and the lack of a comparable trend in the heat flow data.

recharge there (Figure 8c, short-dashed curve). This model predicts elevated heat flow at the fault trace, where upward groundwater flow is locally increased by high permeability, as well as to the northeast of the fault trace, where modeled heat flow is consistently 30–40 mW m^{-2} larger than observed. For a damage zone permeability of 10^{-15} m^2, modeled heat flow is depressed to the southwest of the fault, and is significantly elevated to distances ~30 km northeast of the fault, where modeled values are consistently greater than observed values by ~30–40 mW m^{-2}. For all of the fault zone permeability scenarios we examined, models that incorporate frictional heating along a strong fault are inconsistent with the heat flow data, whereas a range of models that incorporate heat production along a weak fault are consistent with observations.

4.4. Patterns of Heat Flow and Elevation

[33] In regions characterized by high recharge rates, near-surface thermal gradients are typically depressed at high elevations as a result of regional groundwater recharge, and increased at low elevations as a result of groundwater discharge [e.g., *Bredehoeft and Papadopulos*, 1965; *Smith and Chapman*, 1983]. In our simulations, modeled heat flow decreases systematically with increasing elevation for high-permeability scenarios in both the Mojave and Parkfield areas, from values as high as 150–200 mW m^{-2} at the lowest elevations to nearly zero at the highest elevations (Figures 9a–9b). In contrast, conduction-dominated heat transport results in only a slight decrease (20 mW m^{-2}) in heat flow between the lowest and highest elevations. Existing heat flow observations, although primarily collected at intermediate elevations, do not vary significantly with elevation (Figures 9a–9b), suggesting that heat transport is dominated by conduction. Although our highest permeability models are consistent with an upper limit on recharge of 7–10% of annual precipitation, we note that the available recharge in arid regions may be considerably smaller than this. An upper limit on recharge of 1% of annual precipitation is consistent with our model scenarios for homogeneous permeability $<10^{-16}$ m^2 and dominantly conductive heat transport. The interpretation of dominantly conductive heat transport is further supported by (1) low measured in situ permeabilities of $0.5–1.7 \times 10^{-18}$ m^2 at the Cajon Pass borehole [*Coyle and Zoback*, 1988], (2) linear thermal profiles in most observation boreholes, interpreted by *Lachenbruch and Sass* [1980] and *Sass et al.* [1997] to indicate negligible advective disturbance of heat flow, and (3) the fact that temperatures projected from shallow measurements assuming conductive heat flow are consistent with the maximum depth of observed seismicity [e.g., *Sass et al.*, 1997].

5. Implications and Additional Considerations

[34] At Parkfield, models that incorporate frictional heating along either a strong or a weak San Andreas Fault are consistent with observed heat flow, depending on assumed permeability (Figures 4 and 5). In the Mojave region, for a wide range of plausible steady state groundwater flow scenarios, predicted heat flow patterns are inconsistent with frictionally generated heating along a strong fault. In contrast, models that incorporate frictional heating along a weak fault are consistent with observed heat flow values, for a wide range of hydrologic scenarios (Figures 4–8).

[35] The basal heat flux used in our models is based on average observed values that are part of a broadly distributed high heat flow anomaly in the California Coast Ranges [e.g., *Lachenbruch and Sass*, 1980]. It is important to note that the cause of this high regional heat flow is not well understood. High heat flow throughout the California Coast Ranges has been interpreted as a transient thermal response to the migration of the Mendocino Triple Junction and associated slab window [*Lachenbruch and Sass*, 1980; *Guzofski and Furlong*, 2002]. Alternatively, *Lachenbruch and Sass* [1980] and *Scholz* [2000] note the possibility that the regionally high heat flow could reflect lower basal heat flux, combined with broadly redistributed frictionally generated heat from a strong SAF. Regardless of the choice of basal heat flux, for all of the hydrologic scenarios we examined models that incorporate heating along a strong fault predict systematic differences in heat flow with distance from the fault trace or with elevation (for homogeneous $k = 10^{-15}$ m^2) that are not observed.

[36] Models that incorporate heating along a strong fault, and in which advective disturbance is minimal (permeability $<10^{-15}$ m^2), or is localized to shallow depths, predict a distinctive pattern of significantly higher heat flow near the

fault trace than at distances >15 km. This pattern is clearest to the northeast of the fault, where most heat flow data are sited. As noted by *Lachenbruch and Sass* [1980] and as shown in detail here, such a pattern is inconsistent with observed heat flow. Similarly, models in which significant advection is localized along a permeable damage zone predict a heat flow pattern for heating along a strong fault that is inconsistent with observations, whereas model predictions for heating along a weak fault are consistent with the data. For a highly permeable fault zone, advective effects on near-surface heat flow are generally only expected at the fault trace (e.g., Figure 7), regardless of fault dip [e.g., *Forster and Smith*, 1988; *Lopez and Smith*, 1995]. Thus near-surface heat flow patterns for a steeply dipping fault should be essentially the same as for a vertical fault.

[37] In cases where advection is significant (permeability $\geq 10^{-15}$ m^2), the pattern of decreasing heat flow with distance from the fault is less apparent (Figures 4c–4d and 5b, red curves), although modeled values within ~25 km of the fault trace are ~30 mW m^{-2} greater than modeled values beyond this distance. Moreover, these models predict a strong relationship between heat flow and elevation (Figure 9), which is not observed.

[38] Our modeling results do not rule out the possibility of along-strike fluid and heat transport within or near the fault plane itself [e.g., *Lopez and Smith*, 1995]. Such a mechanism would require a highly permeable fault or damage zone, as well as significant along-strike topographic relief to drive flow. We note that such focused along-fault fluid transport would result in elevated heat flow and fluid discharge at topographic lows along the fault trace. The facts that such a pattern is generally not observed [e.g., *Lachenbruch and Sass*, 1980], and that springs associated with the San Andreas itself are rare [e.g., *Kharaka et al.*, 1999] imply that such along-fault flow is not significant. This conclusion is supported by the observation that topographic relief along the SAF adjacent to our Mojave Desert profiles is generally very low when compared to relief perpendicular to the fault (Figure 1b).

[39] Our results demonstrate that steady state, topographically driven groundwater flow is an unlikely mechanism for redistribution of frictionally generated heat along a strong fault. At this stage, we cannot rule out the possibility that heat generation and groundwater flow are both transient and related to the earthquake cycle. This process is unlikely along creeping sections of the fault, but remains an alternative along seismically active fault segments. Enhanced permeability following large earthquakes [e.g., *Rojstaczer and Wolf*, 1992] may provide a mechanism for rapid transient heat advection. Specifically, it is possible that heating occurs during earthquake slip, and fluids then advect the frictionally generated heat toward the Earth's surface through newly formed highly permeable fractures in the postseismic period. Observations of significant fluid discharge at the surface following seismic activity are rare (see discussion by *Lachenbruch and Sass* [1980]); however, if fluids discharge into highly active shallow aquifer units rather than to the Earth's surface, the advected heat could remain undetected without heat flow or water temperature measurement at the appropriate locations and times. Repeated shallow heat flow observations near the fault trace, combined with additional modeling work, are clearly needed to evaluate this hypothesis.

6. Conclusions

[40] In the Mojave region, we find that for a wide range of permeability scenarios, models that incorporate frictional heating from a strong fault are inconsistent with existing heat flow data. In comparison, weak fault heating models for the Mojave region are consistent with observed heat flow for all cases, with the exception of homogeneous high permeability of 10^{-15} m^2. Our results also demonstrate that the lack of an observed frictional heat flow anomaly in the Mojave area cannot be readily explained by along-strike topographic variability (Figure 6), or by steady state fluid flow discharging to active valley groundwater basins (Figure 7). Thus our analysis supports previous interpretations of the heat flow data and suggests that the San Andreas Fault adjacent to the Mojave Desert is, indeed, anomalously weak. In the Parkfield region, existing heat flow data do not clearly distinguish between frictional heating from a strong and a weak San Andreas Fault given the location of existing heat flow stations, and the uncertainty in comparing model results with the heat flow data. In both regions, significant advective heat transport should result in a distinct pattern of decreasing heat flow with increasing elevation; the fact that observed heat flow does not follow this trend implies that heat transport is dominated by conduction. Future work is needed to quantitatively evaluate the possibilities of transient or along-strike or fluid and heat transport, as well as to more comprehensively evaluate the possibility that moderate fault strength or variable basal heat flux may be consistent with observed heat flow.

[41] **Acknowledgments.** We thank Art Lachenbruch, Colin Williams, David Chapman, and Rob Harris for helpful discussions during the course of this work and Art Lachenbruch and Ward Sanford for careful reviews of an early version of this manuscript. We also thank David Castillo and Chris Scholz for their helpful reviews. This work was supported by a National Research Council postdoctoral associateship to Saffer and by NSF grant EAR-0125189 to Saffer.

References

Birch, F., Flow of heat in the Front Range, Colorado, *Geol. Soc. Am. Bull.*, *61*, 567–630, 1950.

Blackwell, D. D., J. L. Steele, and C. A. Brott, The terrain effect on terrestrial heat flow, *J. Geophys. Res.*, *85*, 4757–4772, 1980.

Bredehoeft, J. D., and I. S. Papadopulos, Rates of vertical groundwater movement estimated from the Earth's thermal profile, *Water Resour. Res.*, *1*, 325–328, 1965.

Brune, J. N., T. L. Henyey, and R. F. Roy, Heat flow, stress, and rate of slip along the San Andreas fault, California, *J. Geophys. Res.*, *74*, 3821–3827, 1969.

Byerlee, J. D., Friction of rocks, *Pure Appl. Geophys.*, *116*, 615–629, 1978.

Caine, J. S., J. P. Evans, and C. B. Forster, Fault zone architecture and permeability structure, *Geology*, *24*, 1025–1028, 1996.

Coyle, B., and M. D. Zoback, In situ permeability and fluid pressure measurements at ~2 km depth in the Cajon Pass research well, *Geophys. Res. Lett.*, *15*, 1029–1032, 1988.

Durbin, T. J., Calibration of a mathematical model of the Antelope Valley groundwater basin, California, *U.S. Geol. Surv. Water Supply Pap.*, *2046*, 51 pp., 1978.

Ellsworth, W. L., Earthquake history, 1769–1989, in *The San Andreas Fault System, California*, edited by R. E. Wallace, *U.S. Geol. Soc. Prof. Pap.*, *1515*, 153–187, 1990.

Forster, C., and L. Smith, Groundwater flow systems in mountainous terrain: 2. Controlling factors, *Water Resour. Res.*, *24*, 1011–1023, 1988.

Fuis, G., et al., Crustal structure and tectonics from the Los Angeles basin to the Mojave Desert, southern California, *Geology*, *29*, 15–18, 2001.

Galloway, D. L., et al., Detection of aquifer system compaction and land subsidence using interferometric synthetic aperture radar, Antelope Valley, Mojave Desert, California, *Water Resour. Res.*, *34*, 2573–2585, 1998.

Griscom, A., and R. C. Jachens, Crustal and lithospheric structure from gravity and magnetic studies, in *The San Andreas Fault System, California*, edited by R. E. Wallace, *U.S. Geol. Soc. Prof. Pap.*, *1515*, 239–259, 1990.

Guzofski, C. A., and K. P. Furlong, Migration of the Mendocino triple junction and ephemeral crustal deformation: Implications for California Coast range heat flow, *Geophys. Res. Lett.*, *29*(1), 1012, doi:10.1029/2001GL013614, 2002.

Hardebeck, J. L., and E. Hauksson, Role of fluids in faulting inferred from stress field signatures, *Science*, *285*, 236–239, 1999.

Hickman, S. H., Stress in the lithosphere and the strength of active faults, *U.S. Natl. Rep. Int. Union Geod. Geophys., Rev. Geophys., Suppl.*, 759–775, 1991.

Hill, D. P., J. P. Eaton, and L. M. Jones, Seismicity: 1980–86, in *The San Andreas Fault System, California*, edited by R. E. Wallace, *U.S. Geol. Soc. Prof. Pap.*, *1515*, 115–151, 1990.

Ingebritsen, S. E., and C. E. Manning, Geological implications of a permeability-depth curve for the continental crust, *Geology*, *27*, 1107–1110, 1999.

Jones, L. M., Focal mechanisms and the state of stress on the San Andreas fault in southern California, *J. Geophys. Res.*, *93*, 8869–8891, 1988.

Kharaka, Y. K., et al., Geochemistry and hydromechanical interaction of fluids associated with the San Andreas Fault System, California, in *Faults and Subsurface Fluid Flow in the Shallow Crust*, *Geophys. Monogr. Ser.*, vol. 113, edited by W. C. Haneberg et al., pp. 129–148, AGU, Washington, D. C., 1999.

Lachenbruch, A. H., and J. H. Sass, Thermo-mechanical aspects of the San Andreas Fault system, in *Conference on Tectonic Problems of the San Andreas Fault System, Proceedings*, *Stanford Univ. Publ. Geol. Sci.*, *13*, 192–205, 1973.

Lachenbruch, A. H., and J. H. Sass, Heat flow and energetics of the San Andreas fault zone, *J. Geophys. Res.*, *85*, 6185–6222, 1980.

Lachenbruch, A. H., and J. H. Sass, Heat flow from Cajon Pass, fault strength, and tectonic implications, *J. Geophys. Res.*, *97*, 4995–5015, 1992.

Lachenbruch, A. H., et al., Heat flow at Cajon Pass, California, revisited, *J. Geophys. Res.*, *100*, 2005–2012, 1995.

Lopez, D. L., and L. Smith, Fluid flow in fault zones: Analysis of the interplay of convective circulation and topographically driven groundwater flow, *Water Resour. Res.*, *31*, 1489–1503, 1995.

Mount, V. S., and J. Suppe, State of stress near the San Andreas Fault; implications for wrench tectonics, *Geology*, *15*, 1143–1146, 1987.

O'Neil, J. R., and T. C. Hanks, Geochemical evidence for water-rock interaction along the San Andreas and Garlock faults of California, *J. Geophys. Res.*, *85*, 6286–6292, 1980.

Oppenheimer, D. H., P. A. Reasenberg, and R. W. Simpson, Fault-plane solutions for the 1984 Morgan Hill, California earthquake sequence: Evidence for the state of stress on the Calaveras fault, *J. Geophys. Res.*, *93*, 9007–9026, 1988.

Planert, M., and J. S. Williams, Ground water atlas of the United States, Segment 1 California, Nevada, *U.S. Geol. Surv. Hydrol. Invest. Atlas 730-B*, 28 pp., 1995.

Rojstaczer, S., and S. Wolf, Permeability changes associated with large earthquakes: An example from Loma Prieta, California, *Geology*, *20*, 211–214, 1992.

Sass, J. H., et al., An analysis of thermal data from the vicinity of Cajon Pass, California, *U.S. Geol. Surv. Open File Rep., 86–468*, 47 pp., 1986.

Sass, J. H., et al., Heat flow from a scientific research well at Cajon Pass, California, *J. Geophys. Res.*, *97*, 5017–5030, 1992.

Sass, J. H., et al., Thermal regime of the San Andreas fault near Parkfield, California, *J. Geophys. Res.*, *102*, 27,575–27,585, 1997.

Scholz, C., Evidence for a strong San Andreas fault, *Geology*, *28*, 163–166, 2000.

Smith, L., and D. S. Chapman, On the thermal effects of groundwater flow: 1. Regional scale systems, *J. Geophys. Res.*, *88*, 593–608, 1983.

Thurber, C., et al., Two-dimensional seismic image of the San Andreas Fault in the northern Gabilan Range, central California: Evidence for fluids in the fault zone, *Geophys. Res. Lett.*, *24*, 1591–1594, 1997.

Townend, J., and M. D. Zoback, How faulting keeps the crust strong, *Geology*, *28*, 399–402, 2000.

Townend, J., and M. D. Zoback, Implications of earthquake focal mechanisms for the frictional strength of the San Andreas Fault system, in *The Nature and Tectonic Significance of Fault Zone Weakening*, edited by R. E. Holdsworth, R. A. Strachan, J. F. Magloughlin, and R. J. Knipe, *Geol. Soc. Spec. Publ.*, *186*, 13–21, 2001.

Unsworth, M., et al., Along strike variations in the electrical structure of the San Andreas Fault at Parkfield, California, *Geophys. Res. Lett.*, *27*, 3021–3024, 2000.

Voss, C. I., A finite element simulation model for saturated-unsaturated, fluid density-dependent groundwater flow with energy transport or chemically reactive single-species solute transport: *U.S. Geol. Surv. Water Resour. Invest. Rep., 84–4369*, 1984.

Williams, C. F., and T. N. Narisimhan, Hydrogeologic constraints on heat flow along the San Andreas Fault: A testing of hypotheses, *Earth Planet. Sci. Lett.*, *92*, 131–143, 1989.

Zoback, M. D., and G. C. Beroza, Evidence for near-frictionless faulting in the 1989 (*M*6. 9) Loma Prieta, California, earthquake and its aftershocks, *Geology*, *21*, 181–185, 1993.

Zoback, M. D., et al., New evidence on the state of stress of the San Andreas fault system, *Science*, *238*, 1105–1111, 1987.

B. A. Bekins, U.S. Geological Survey, 345 Middlefield Road, MS 946, Menlo Park, CA 94025, USA. (babekins@usgs.gov)

S. Hickman, U.S. Geological Survey, 345 Middlefield Road, MS 977, Menlo Park, CA 94025, USA. (hickman@usgs.gov)

D. M. Saffer, Department of Geology and Geophysics, University of Wyoming, Laramie, WY 82071-3006, USA. (DSaffer@uwyo.edu)